Supporting Information for:

The Crystal Structure of a High-Spin OxoIron(IV) Complex and Characterization of Its Self-Decay Pathway.

Jason England,[†] Yisong Guo,[‡] Erik R. Farquhar,[†] Victor J. Young, Jr.,[†] Eckard Münck,[*,‡] and Lawrence Que, Jr.[*,†]

Contents:

Figure S1. ESI-MS of the self-decay products of **1**. (**A**) and (**B**) correspond to mixtures of the dicationic and monocationic fragments $[Fe^{III}(O)(L - H)]^{2+}$ and $[Fe^{III}(OH)(L)]^{2+}$, and $\{[Fe^{III}(O)(L - H)](OTf)\}^{+}$ and $\{[Fe^{III}(OH)(L)](OTf)\}^{+}$, respectively. The experimentally observed data (black bars) was fit as 60 % $\{[Fe^{III}(O)(L - H)](OTf)\}^{+}$ and $[Fe^{III}(O)(L - H)]^{2+}$ and 40 % $\{[Fe^{III}(OH)(L)](OTf)\}^{+}$ and $[Fe^{III}(OH)(L)]^{2+}$ (red bars). (**C**) and (**D**) result from self-decay of ^{18}O-labelled **1**. The experimentally observed data (black bars) was fit as 10 % $\{[Fe^{III}(^{16}O)(L - H)](OTf)\}^{+}$ and $[Fe^{III}(^{16}O)(L - H)]^{2+}$, 70 % $\{[Fe^{III}(^{18}O)(L - H)](OTf)\}^{+}$ and $[Fe^{III}(^{18}O)(L - H)]^{2+}$ and 20 % $\{[Fe^{III}(^{18}OH)(L)](OTf)\}^{+}$ and $[Fe^{III}(^{18}OH)(L)]^{2+}$ (red bars). All solutions were prepared by reaction of 3 mM CH_3CN solutions of **2** at -30°C with either 1 equiv $^{t}BuSO_2PhIO$ or $^{t}BuSO_2PhI^{18}O$, to yield **1**, which was then allowed to undergo self-decay by warming to 25°C. All reactions were monitored by UV-Vis spectroscopy and all ESI-MS peak intensities were normalized according to the most intense peak in the corresponding ion fragment.

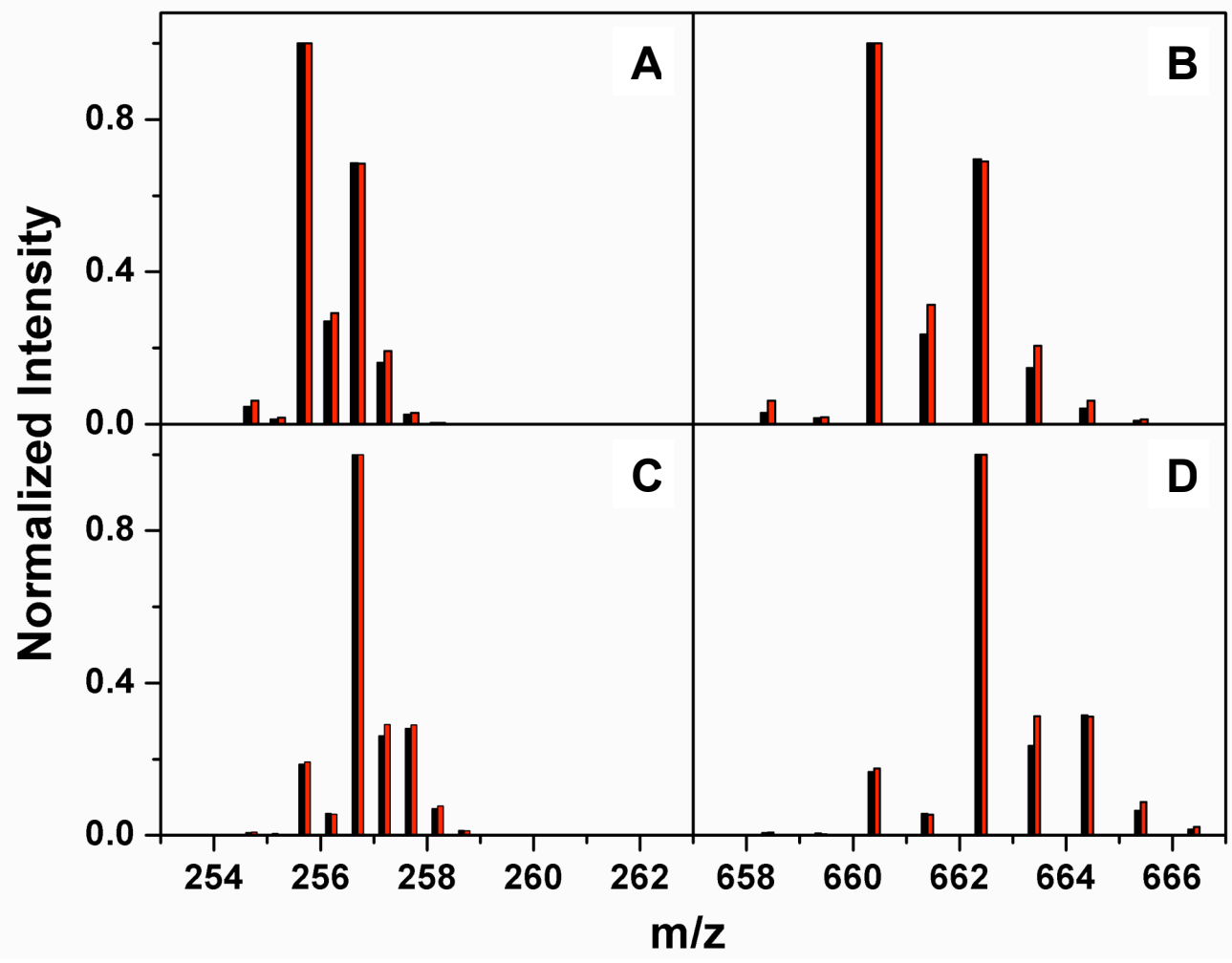

Figure S2. ESI-MS of the products of reaction of **1** with 1,4-cyclohexadiene (1,4-CHD). (**A**) and (**B**) correspond to fragments $[Fe^{III}(OH)(L)]^{2+}$ and $\{[Fe^{III}(OH)(L)](OTf)\}^{+}$, respectively. Experimentally observed data = black bars; calculated isotope distribution = red bars. (**C**) and (**D**) result from reaction of ^{18}O-labelled **1** with 1,4-CHD. The experimentally observed data (black bars) was fit as 16 % $[Fe^{III}(^{16}OH)(L)]^{2+}$ and $\{[Fe^{III}(^{16}OH)(L)](OTf)\}^{+}$, and 84 % $\{[Fe^{III}(^{18}OH)(L)](OTf)\}^{+}$ and $[Fe^{III}(^{18}OH)(L)]^{2+}$ (red bars). All solutions were prepared by reaction of 3 mM CH_3CN solutions of **2** at -30°C with either 1 equiv $^{t}BuSO_2PhIO$ or $^{t}BuSO_2PhI^{18}O$, to yield **1**, which was then reacted with approximately 40 equiv of 1,4-CHD. All reactions were monitored by UV-Vis spectroscopy and all ESI-MS peak intensities were normalized according to the most intense peak in the corresponding ion fragment.

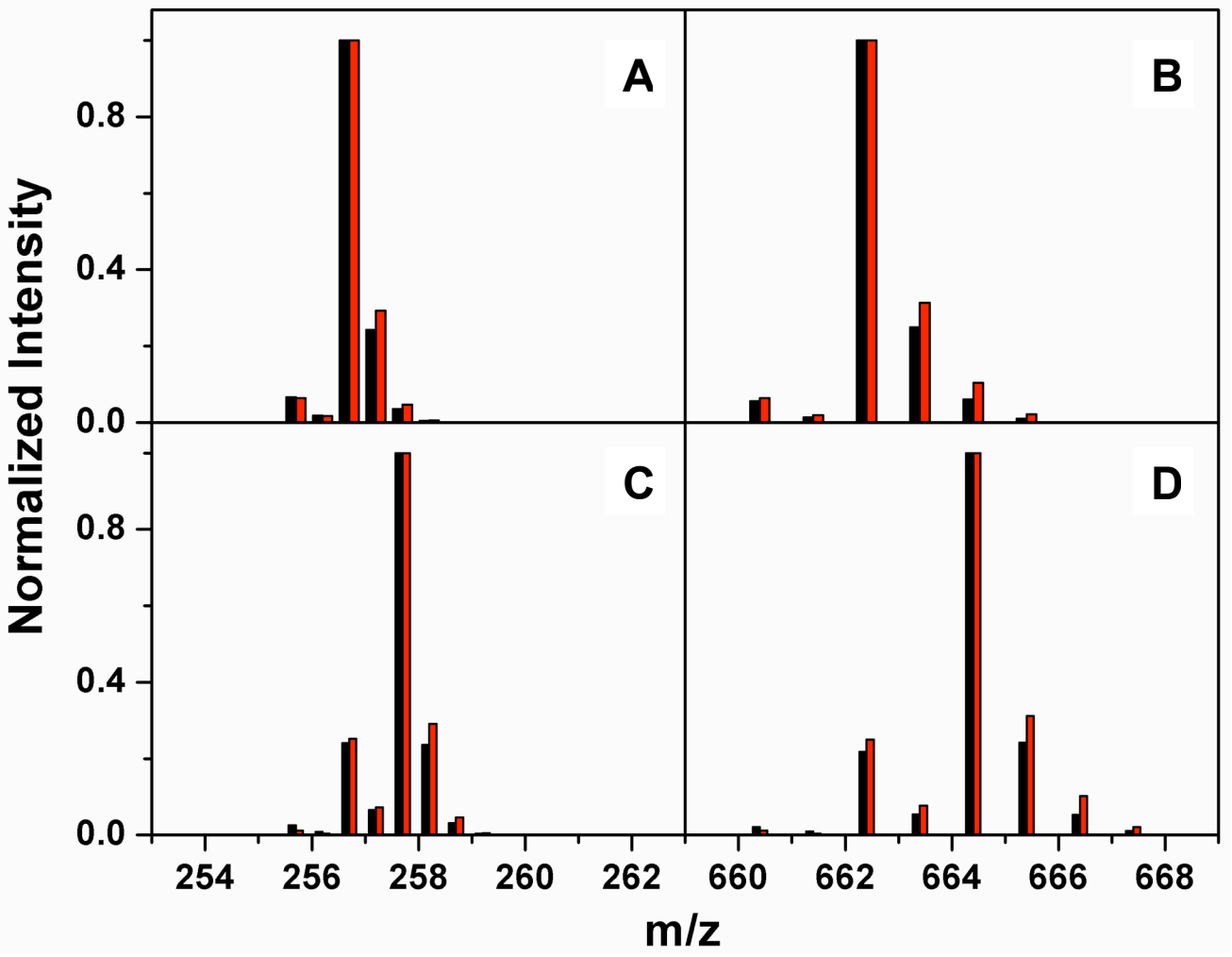

Figure S3. X-band EPR spectrum of the product of reaction of **1** with 1,4-CHD (black line), recorded at 2.3 K, and simulated spectrum for an S = 3/2 component (red line). The parameters used were D = -6 cm-1, E/D = 0.22, $\sigma_{E/D}$ = 0.025, g_x = 2, g_y = 2.06, g_z = 2.14. Conditions: frequency 9.62 GHz; microwave power 0.2 mW; modulation amplitude 1 mT.

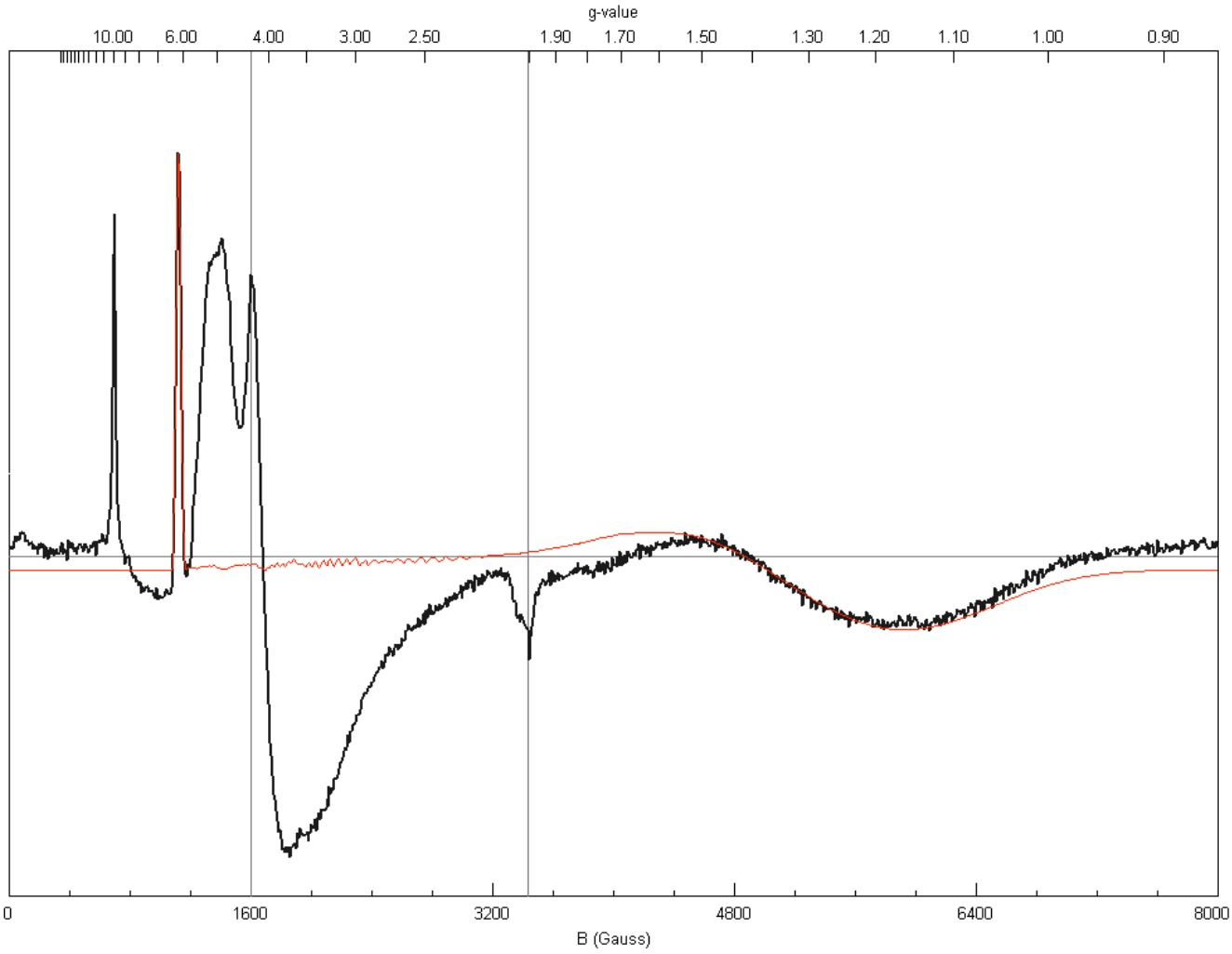

Figure S4. The pseudo-first order rate of decay of the NIR bands, at 825 and 865 nm, associated with **d_{36}-1** (k_{eff}), as a function of THF (black triangles) and THF-d_8 (red circles) concentration. These reactions were performed using 2 mM CH_3CN solutions of **d_{36}-1**, under an inert atmosphere, at 0°C.

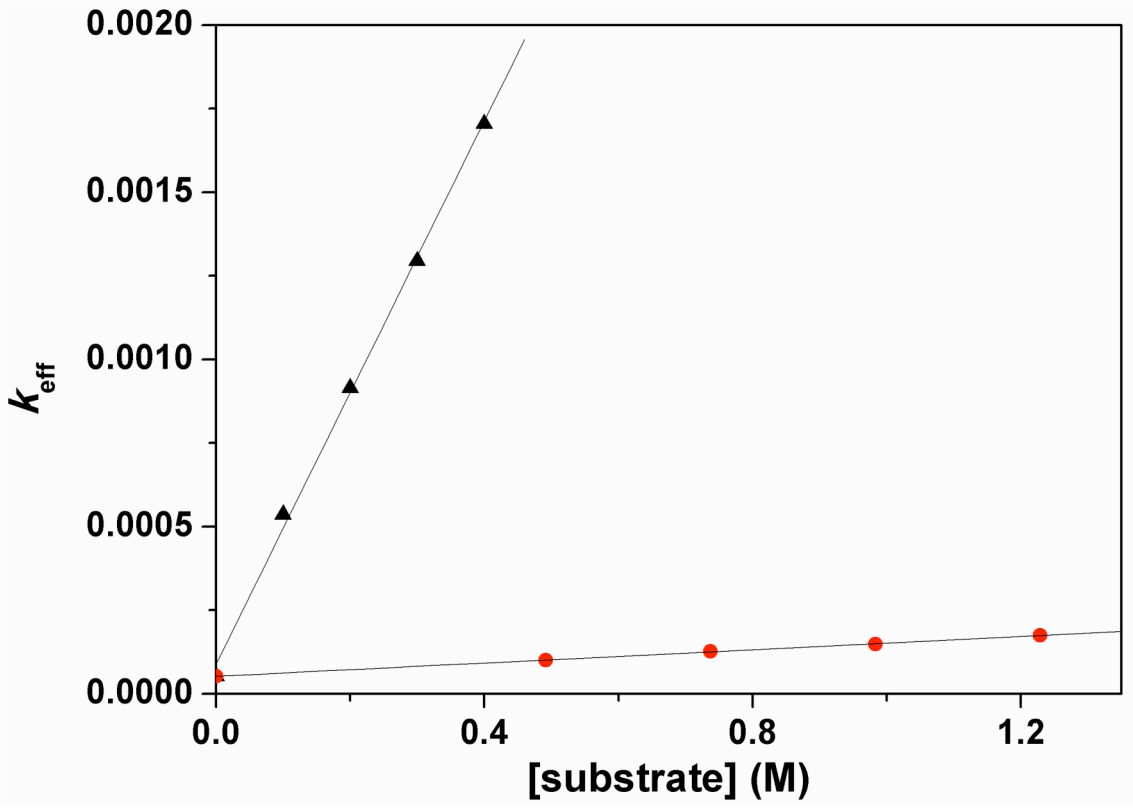

$$d[Fe^{IV}(O)]/dt = -k_{eff}[Fe^{IV}(O)]$$

$$k_{eff} = k_{sd} + k_2[substrate]$$

where,

k_{sd} = rate of self-decay of **d_{36}-1**

k_2 = second order rate constant for reaction of **d_{36}-1** with substrate

Hence, the slope of the linear fit to the increase in k_{eff} as a function of substrate concentration yields second order rate constants, k_2, of 4.1×10^{-3} and 9.9×10^{-5} M^{-1} s^{-1} for THF and THF-d_8, respectively (KIE = 40). The intercepts on the y-axis correspond to k_{sd}.

Figure S5. (**A**) Thermal ellipsoid drawing of $[Fe^{IV}(O)(TMG_3tren)]^{2+}$ (**d_{36}-1**), based upon 50% probability ellipsoids, showing the view down the Fe=O axis. Dashed lines indicate close C-D···O non-bonded contacts. Counterions, ^{1}H atoms and solvent molecules have been omitted for clarity. (**B**) Thermal ellipsoid drawing of $[Fe^{IV}(O)(TMC)(CH_3CN)]^{2+}$ (**3**), showing 50% probability ellipsoids. Dashed lines indicate close C-H···O non-bonded contacts. Counterions and solvent molecules have been omitted for clarity. Atom color scheme: C, gray; H, white; N, blue, O, red; Fe, magenta.

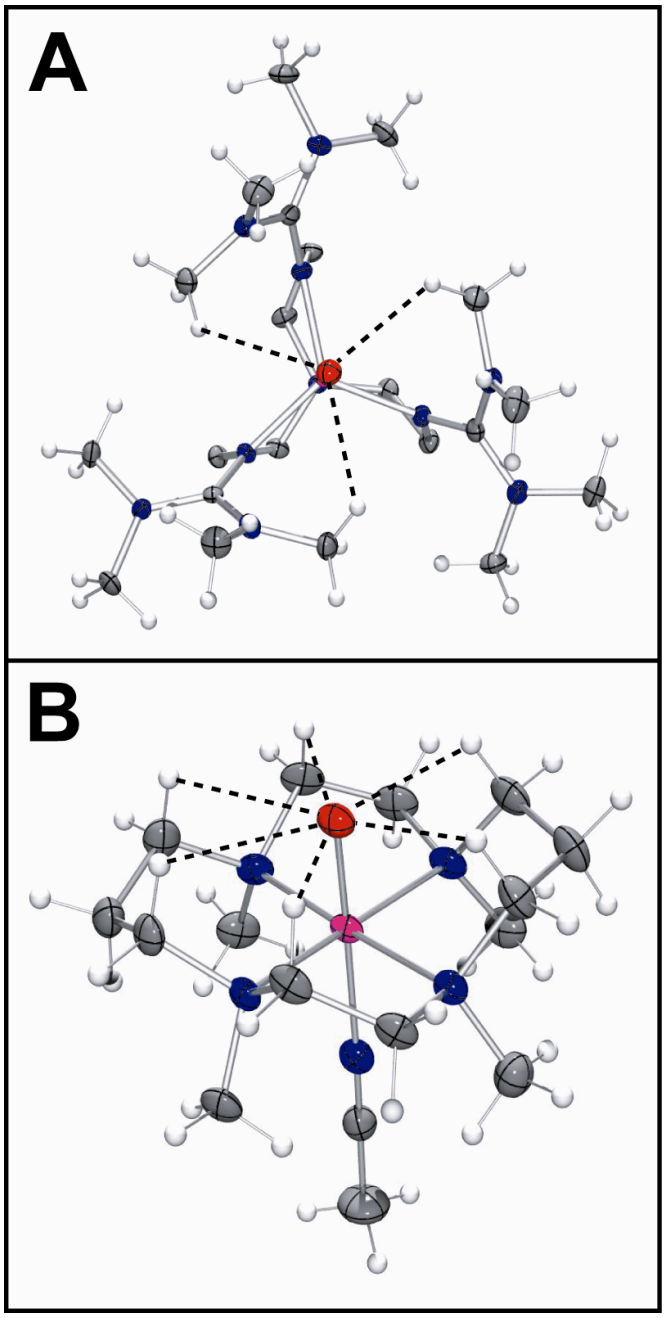

X-ray Absorption Spectroscopic Analysis of D

Data reduction, averaging, and normalization were performed using the program EXAFSPAK.[1] Following calibration and averaging of the data, background absorption was removed by fitting a Gaussian function to the pre-edge region and then subtracting this function from the entire spectrum. A three-segment spline with fourth order components was then fit to the EXAFS region of the spectrum in order to extract $\chi(k)$, using spline points obtained with the program PySpline.[2] Analysis of the pre-edge features was carried out with the program SSExafs[3] using a previously reported method.[4] In all EXAFS fits of **D**, the coordination number *n* of a given shell was a fixed parameter, and was varied iteratively while r and σ^2 were allowed to freely float. The amplitude reduction factor S_0 was fixed at 0.9, while the edge shift parameter E_0 was allowed to float at a common value for all shells. Phase and amplitude parameters were calculated using FEFF 8.40 [5] at the single-scattering level of theory, and these parameters were utilized by the 'opt' program of the EXAFSPAK package during curve-fitting. The FEFF input coordinates consisted of a modification of the structure of **1** in which the Fe–O bond length was lengthened to 1.825 Å while other atomic positions were unchanged. For purposes of quantifying fit quality, the goodness-of-fit parameter *F* was defined as $[\Sigma k^6(\chi_{exptl}-\chi_{calc})^2 / \Sigma k^6\chi_{exptl}^2]^{1/2}$. A second criterion, *F*', was used to investigate the effect that additional variables have on improving the fit, and was thus used to compare fits with differing numbers of shells. *F*' is defined as $F' = F^2 / N_{IDP} - \rho$, where $N_{IDP} = 2\Delta k\Delta R/\pi$, and ρ is the number of floating variables in the fit.[6]

During data collection, a modest red-shift in the position of the rising Fe K-edge was observed, and so at least three scans were collected for each of three different spots on the sample. Analysis of single scans indicated a red-shift of at most 0.2 – 0.25 eV for the third scan relative to the first scan at each spot, based on the zero-crossing point of the second derivative of the data. The first and third scans exhibited identical pre-edge intensities and $k^3\chi(k)$ EXAFS spectra. The observed putative photoreduction was therefore deemed insignificant, and the XANES and EXAFS analyses presented herein reflect the summed average of the first three scans over the three exposed spots on the sample (9 total scans). EXAFS analysis of the sum of first scan data gave a best fit identical to that presented below.

Figure S6 shows a comparison of $k^3\chi(k)$ EXAFS data and its Fourier transformation for **D** with the published data[7] for the oxoiron(IV) precursor **1**. The amplitude of the EXAFS oscillations for **D** is smaller than that of **1**, and this manifests quite clearly in the Fourier transformation.

Specifically, the outer shell peaks are of similar intensities for **1** and **D**, while the inner shell peak of **D** is considerably less intense and somewhat broadened relative to **1**. This observation is indicative of a greater degree of destructive overlap in the EXAFS oscillations associated with the inner shell of **D**, due to either the specific combination of bond lengths or greater static disorder in the range of bond lengths.

Table S2 enumerates the fitting protocol for a sample of **D** shown to be 88% Fe(III) by Mössbauer analysis prior to XAS measurements. The inner shell can be modeled as a shell of Fe–N scatterers at 2.00 Å corresponding to the equatorial nitrogen donors of the TMG_3tren ligand. Addition of a short Fe–O/N scatterer at *ca*. 1.77 Å to the fit leads to an improved goodness-of-fit and visual agreement with experimental data, particularly in the Fourier transform. We assign this short Fe–O/N distance to the Fe(III)–OH moiety. Addition of a longer Fe–N shell corresponding to the axial Fe–N interaction affords decreases in fit quality and unreasonably large σ^2 values (fits 7a,b), indicating that this shell is not a required component of the fit. The outer-shell features can be modeled with two distinct shells of Fe•••C scatterers attributable to the backbone of the TMG_3tren ligand, and consistent with our previously published EXAFS analysis with the oxoiron(IV) precursor of **D**.[7] The requirement for a short Fe–OH distance to obtain good fits is illustrated in Figure S7 as a comparison of fit 21, in which the short Fe–O/N shell is absent, to the best fit, fit 14, in which it is present. Fit 21 exhibits a significant mismatch between the calculated and experimental Fourier transforms (particularly for the inner shell) and in the amplitudes of the $k^3\chi(k)$ EXAFS that is ameliorated by the addition of the 1.77 Å shell to afford fit 14.

Figure S7. (left) Comparison of the $k^3\chi(k)$ EXAFS spectra of **D** (——) with its precursor **1** (——). The spectra are scaled identically. (right) Overlay of the Fourier transforms of $k^3\chi(k)$ EXAFS data for **D** (——) and its precursor **1** (——). Fourier transformation ranges are as follows: k = 2-12.15 Å^{-1} (**D**); k = 2-13.3 Å^{-1} (**1**).

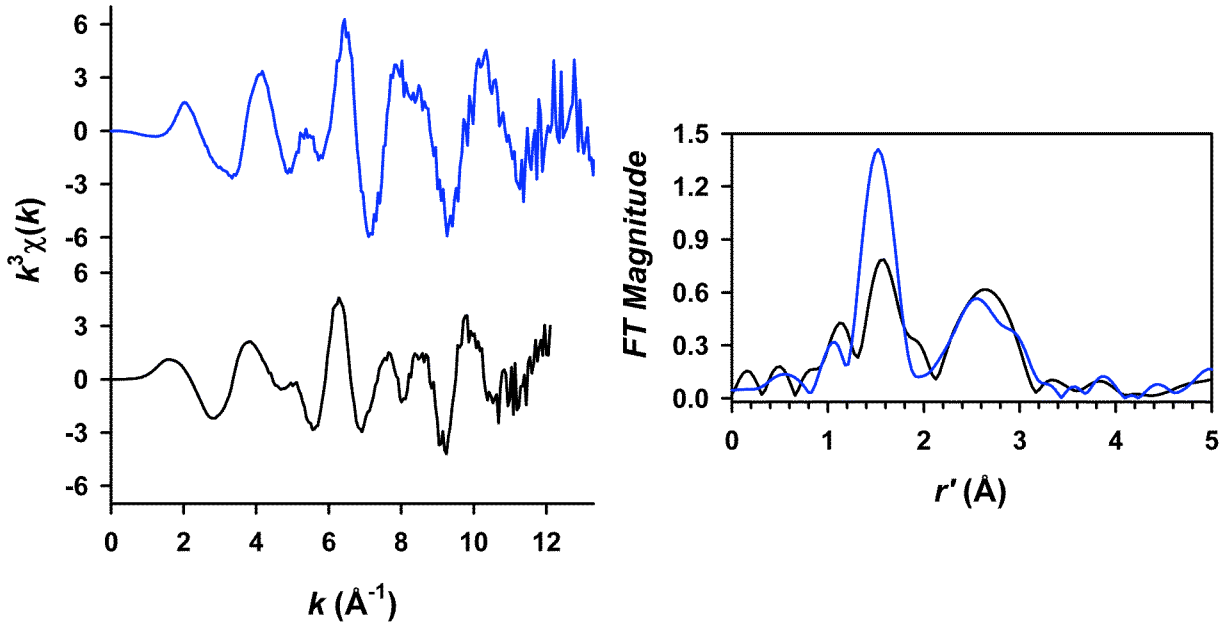

Table S1. Pre-edge analysis parameters for species **D**.[a]

Species	E_{edge} (eV)	$E_{pre\text{-}edge}$ (eV)	height	width	area [b]
D	7122.62	7113.99(1)	0.0669(7)	2.92(4)	20.8(3)

[a] Values in parentheses represent uncertainties in the last digit for those parameters.
[b] The pre-edge peak area has been normalized to the edge jump and multiplied by 100 for convenience.

Table S2. EXAFS fitting results for **D**.[a]

	Fe-N/O			Fe-O			Fe•••C			Fe•••C/N				
fit	**n**	**r**	**σ^2**	**n**	**r**	**σ^2**	**n**	**r**	**σ^2**	**n**	**r**	**σ^2**	***F***	***F'***
1	2	2.03	1.9										0.711	0.374
2	3	2.02	4.8										0.731	0.396
3	4	2.02	7.9										0.771	0.440
4	5	2.01	11.7										0.812	0.488
5	3	2.00	3.2	1	1.78	6.3							0.692	0.416
5a	3	2.00	3.2	0.9	1.77	5.5							0.692	0.416
6	4	1.99	5.4	1	1.75	4.4							0.699	0.424
6a	4	1.99	5.6	0.9	1.74	3.7							0.698	0.424
7a	3 1	2.008 2.361	3.31 13.22	0.9	1.78	6.4							0.688	0.498
7b	3 1	2.033 2.351	4.82 8.10										0.712	0.440
8	3	2.02	3.4	0.9	1.78	7.2	4	3.02	0.5				0.438	0.202
9	3	2.02	3.3	0.9	1.78	7.3	5	3.02	1.6				0.431	0.196
10	3	2.02	3.4	0.9	1.78	7.3	6	3.02	2.6				0.434	0.198
11	3	2.02	3.4	0.9	1.78	7.3	7	3.02	3.6				0.443	0.207
12	3	2.01	3.3	0.9	1.77	5.8	5	3.00	2.3	5	3.38	3.1	0.299	0.119
13	3	2.00	3.3	0.9	1.77	5.4	5	3.00	2.4	6	3.38	4.1	0.297	0.117
14	***3***	***2.00***	***3.3***	***0.9***	***1.77***	***5.1***	***5***	***2.99***	***2.6***	***7***	***3.37***	***5.0***	***0.295***	***0.116***
15	3	2.00	3.2	0.9	1.77	4.6	5	2.99	2.8	8	3.37	5.7	0.295	0.116
16	3	2.01	3.4	0.9	1.77	5.9	6	3.00	3.6	6	3.38	4.6	0.298	0.118
17	3	2.01	3.3	0.9	1.77	5.7	6	3.00	3.7	7	3.38	5.6	0.296	0.117
18	3	2.00	3.3	0.9	1.77	5.4	6	3.00	3.7	8	3.37	6.4	0.296	0.117
19	3	2.03	4.8				5	3.03	1.6				0.467	0.190
20	3	2.02	3.4	0.9	1.78	7.4	5	3.02	1.6				0.431	0.196
21	*3*	*2.02*	*4.9*				*5*	*3.03*	*2.0*	*7*	*3.41*	*7.9*	*0.385*	*0.156*
22	3	2.00	3.3	0.9	1.77	5.1	5	2.99	2.6	7	3.37	5.0	0.295	0.116

[a] Fourier transform range k = 2.0 – 12.15 Å^{-1} (resolution = 0.156 Å). r is in units of Å; σ^2 is in units of 10^{-3} Å^2. All fits are to unfiltered data.

[b] Goodness-of-fit parameter F defined as $[\Sigma k^6(\chi_{exptl}-\chi_{calc})^2 / \Sigma k^6\chi_{exptl}^2]^{1/2}$.

[c] F' = F^2 / ν, where $\nu = N_{IDP} - \rho$. N_{IDP} is the number of independent data points, while ρ is the number of floated variables in each optimization step. The values of F' shown have been multiplied by a factor of 10 for convenience. F' is a measure of whether an added shell significantly improves the fit.[6]

Figure S8. Fits to the Fourier transforms of the Fe K-edge EXAFS data (left) and unfiltered EXAFS spectra ($k^3\chi(k)$, right) for **D**. Experimental data is shown with dashed lines (- - - -), while fits are shown with solid red lines (——). Fourier transformation range: $k = 2 - 12.15$ Å^{-1}. Fit parameters associated with the stated fit are shown in Table S2.

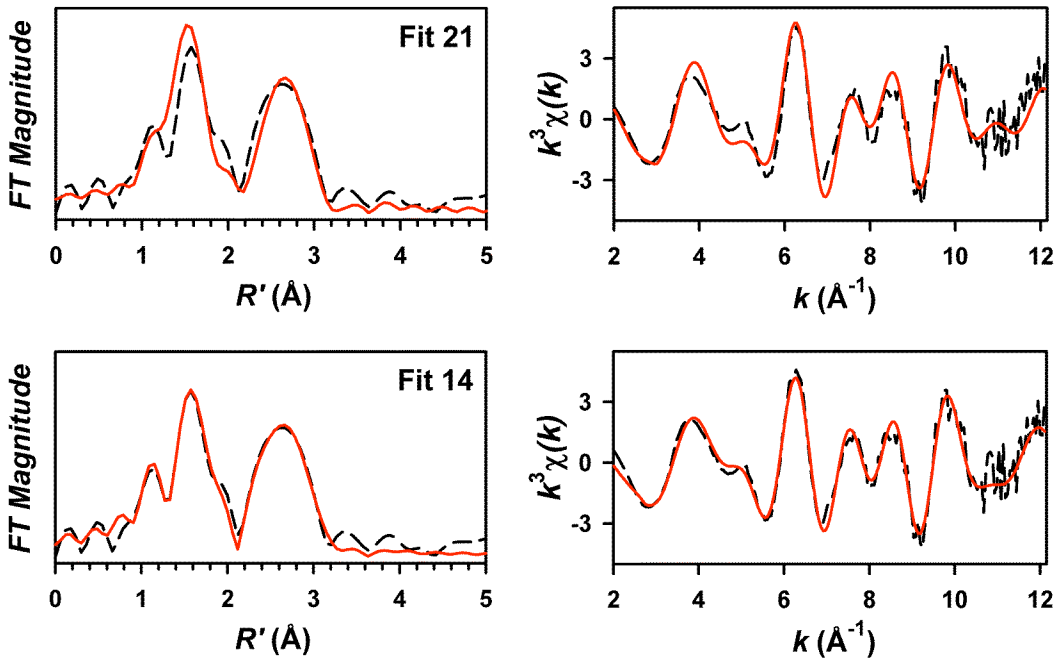

References

1. G. N. George, *EXAFSPAK*; Stanford Synchrotron Radiation Laboratory, Stanford Linear Accelerator Center, Stanford, CA, **2000**.
2. Scarrow, R. C.; Trimitsis, M. G.; Buck, C. P.; Grove, G. N.; Cowling, R. A.; Nelson, M. J. *Biochemistry* **1994**, *33*, 15023.
3. Rohde, J.-U.; Torelli, S.; Shan, X.; Lim, M. H.; Klinker, E. J.; Kaizer, J.; Chen, K.; Nam, W.; Que, L., Jr. *J. Am. Chem. Soc.* **2004**, *126*, 16750.
4. Tenderholt, A.; Hedman, B.; Hodgson, K. O. *AIP Conf. Proc.* **2007**, *882*, 105.
5. Ankudinov, A. L.; Ravel, B.; Rehr, J. J.; Conradson, S. D. *Phys. Rev. B* **1998**, *58*, 7565.
6. Riggs-Gelasco, P. J.; Stemmler, T. L.; Penner-Hahn, J. E. *Coord. Chem. Rev.* **1995**, *144*, 246-286.
7. England, J.; Martinho, M.; Farquhar, E. R.; Frisch, J. R.; Bominaar, E. L.; Munck, E.; Que, L., Jr. *Angew. Chem., Int. Ed.* **2009**, *48*, 3622-3626.